INSTITUTE OF PHYSICS PUBLISHING JOURNAL OF PHYSICS: CONDENSED MATTER

J. Phys.: Condens. Matter **17** (2005) R357–R379 doi:10.1088/0953-8984/17/7/R03

TOPICAL REVIEW

Dielectric properties of crystalline and amorphous transition metal oxides and silicates as potential high-κ candidates: the contribution of density-functional theory

G-M Rignanese

Unité de Physico-Chimie et de Physique des Matériaux, Université Catholique de Louvain, 1 Place Croix du Sud, B-1348 Louvain-la-Neuve, Belgium
and
Research Center on Microscopic and Nanoscopic Materials and Electronic Devices (CERMIN), Université Catholique de Louvain, B-1348 Louvain-la-Neuve, Belgium

E-mail: rignanese@pcpm.ucl.ac.be

Received 22 October 2004, in final form 21 January 2005
Published 4 February 2005
Online at stacks.iop.org/JPhysCM/17/R357

Abstract

A review is given of various first-principles studies of the dielectric properties of crystalline and amorphous transition metal oxides and silicates, which have drawn considerable attention as potential high-κ materials. After a brief summary of the principal equations of density-functional theory related to the dielectric properties of solids, the results obtained for group IVb M = (Hf, Zr, Ti) and IIIb M = (Y, La, Lu) transition metals crystalline oxides and/or silicates are discussed.

For the group IVb transition metals, four crystalline phases (cubic, tetragonal, monoclinic and rutile) of dioxide MO_2 with M = (Hf, Zr, Ti) have been considered in the literature. The results of density-functional theory calculations of the dielectric properties of three crystalline transition metal silicates (hafnon $HfSiO_4$, zircon $ZrSiO_4$ and a hypothetical $TiSiO_4$ structure) are also presented. For the group IIIb transition metals, two crystalline phases (cubic and hexagonal) of sesquioxides M_2O_3 with M = Lu have been investigated within density-functional theory.

Finally, the first-principles results that have been obtained for the amorphous silicates are discussed. A presentation is given of a scheme recently introduced which relates the dielectric constants to the local bonding of Si and metal atoms. It is based on the definition of parameters characteristic of the basic structural units centred on Si and metals atoms and including their nearest O neighbours. Applied to amorphous Zr silicates, it provides a good description of the measured dielectric constants, both of the optical and the static ones.

Contents

1. Introduction

Transition metal oxides (TMOs) constitute a fascinating class of materials of great importance in solid state physics, as well as in materials science. They exhibit a uniquely wide range of electronic properties, which yield a rich field for fundamental research and technological applications.

The main characteristic of TMOs is the incomplete filling of the d shells. The electrons of these orbitals are responsible for an intermediate chemical bonding: neither strongly covalent like for the electrons of the p shells, nor purely metallic like for the electrons of the s shells. Some TMOs have delocalized d bands providing catalytically active surfaces. Others exhibit narrow d bands with emphasized electron correlations giving rise to diverse properties such as high-temperature superconductivity, and colossal magneto-resistance. In contrast to free transition metal atoms or ions, where the d states are degenerate, these levels are energetically split in the oxides due to the crystal field, provided by the surrounding oxygen ions.

Besides, TMOs come in a variety of crystal structures and may individually exhibit several phases. This adds to the variation in the spin, charge and orbital states resulting from the presence of d electrons, to explain the large diversity in the electronic properties and the potential applications of these materials.

TMOs include insulators, metals, semiconductors, and even superconductors. As an example of their fundamental interest, the high-temperature superconductors made from Cu oxides challenge the present understanding of collective electronic behaviour. TMOs are well known for their ferroelectric, antiferroelectric, and piezoelectric properties, which find applications in sensors, actuators and transducers, non-volatile memories, and dynamic random access memories, but also in non-linear optical activity. TMOs can exhibit giant and colossal magneto-resistance. This is mostly the case for Mn oxides, which are at the origin of new applications in magnetic-field sensors. The valence changes of the TMOs form the basis for ionic conductivity, which is the basis for modern batteries and oxygen diffusion. Early glass was often coloured to simulate gemstones by adding transition-metal oxides to the quartz and ash. Cu and Co oxides create shades of blue, Mn oxide produces a purple.

In contrast, transition metal silicates (TMSs) have been much less studied so far, with the notable exception of hafnon ($HfSiO_4$) and zircon ($ZrSiO_4$) which are of great geological significance. They both belong to the orthosilicate class of minerals, which can be found in igneous rocks and sediments. Zircon is used as a gemstone, because of its good optical quality, and resistance to chemical attack. In the earth's crust, hafnon and zircon are host minerals for the radioactive elements uranium and thorium. They have therefore been widely studied in the framework of nuclear waste storage.

Very recently, TMOs and TMSs have attracted considerable attention as alternative high-κ materials to conventional SiO_2 as the gate dielectric in metal–oxide–semiconductor (MOS) transistors. Indeed, the roadmap of the Semiconductor Industry Association [1], which provides the targets for further improvements of MOS devices, indicates that the thickness of SiO_2 (the present gate dielectric) should be smaller than 10 Å, which represents a layer of about five Si atoms across. The use of such a thin SiO_2 layer is precluded by severe leakage problems. Current research is therefore focusing on the replacement of SiO_2 by high-κ materials. The increase of the dielectric constant (κ) compared to SiO_2 permits the use of a gate with a larger physical thickness (t_{phys}) while achieving the same capacitance as devices with a smaller equivalent thickness (t_{eq}) of SiO_2:

$$t_{eq} = \frac{\kappa_{ox}}{\kappa} t_{phys}$$

where κ_{ox} is the dielectric constant of SiO_2. The larger physical thickness solves the potential leakage problems as well as other issues related to the penetration of the gate dopants in the substrate when very thin films are used.

However, replacing the SiO_2 with a material having a different dielectric constant is not as simple as it may seem. The material bulk and interface properties must be comparable to those of silicone dioxide, which are remarkably good. For instance, thermodynamic stability with respect to silicon, stability under thermal conditions relevant to microelectronic fabrication, low diffusion coefficients, and thermal expansion match are quite critical.

With these objectives in mind, group IIIb (Y, La, and to a lesser extent Lu), group IVb (Ti, Zr, and Hf), and group Vb (Ta) transition metal oxides or silicates have been the object of a considerable number of studies as potential high-κ candidates [2]. The group IIIb TMOs in the form of M_2O_3 show many promising and encouraging properties. The beneficial properties of these oxides arise in part because the mole fraction of cations is higher (40 mol%) compared to MO_2 (group IVb) metal oxides, with a cation fraction of 33.3 mol. The group IVb (Ti, Zr and Hf) TMOs and TMs (in the form of MO_2 and $MSiO_4$, respectively) present higher dielectric constants (e.g., 80–110 for TiO_2 depending on the crystal structure), and have therefore generated a considerable amount of investigations. Despite the substantial amount of work that has been reported on Ta_2O_5 as a gate dielectric, the inherent thermal instability when in direct contact with Si is a severe limitation. In fact this criterion has proved crucial in the choice of the next-generation gate dielectrics. In the end, $(HfO_2)_x(SiO_2)_{1-x}$ and $(ZrO_2)_x(SiO_2)_{1-x}$ systems in the form of amorphous films have emerged has the most promising candidates.

In the framework of the quest for high-κ materials to replace conventional SiO_2 as the gate dielectric in MOS devices, first-principles calculations constitute a valuable tool in understanding the behaviour of novel materials at the atomic scale without requiring empirical data. This is particularly interesting for the early stages of research when a relatively small amount of experimental data is available. In terms of its predictive accuracy, density-functional theory (DFT) has proved to be very appropriate for studying the ground-state properties of the electronic system, such as the structural, vibrational, and dielectric properties on which this topical review will focus.

However, DFT has one important drawback associated to the high computational cost of the calculations that are required, which limits both the length and timescales of the phenomena which can be modelled. Nowadays, it is possible to treat systems containing up to hundreds of atoms within the most widespread DFT approach based on plane-wave basis sets and pseudopotentials. For the high-κ materials, it is important to note that transition-metal and first-row elements (e.g. oxygen) generally present an additional difficulty when treated with plane-wave basis sets. Namely, their valence wavefunctions are generally strongly localized

around the nucleus and may require a large number of basis functions to be described accurately, thus further limiting the size of the system that can be investigated.

A number of first-principles studies have been dedicated to high-κ materials [3–27]. However, only a few of these address their dielectric properties [3–11]. Most of the work has focused on group IVb transition metal oxides and silicates. First, the crystalline Zr silicate, namely zircon, was investigated [3]. Next, the tetragonal phase of ZrO_2 was considered [4] and compared to the cubic phase, which had been studied previously for other reasons [13, 14]. The study of the monoclinic phase of ZrO_2 [5] completed nicely the analysis of crystalline Zr oxides. The corresponding work for crystalline Hf oxides was also the object of a thorough study [6]. Recently, a comparison between Hf and Zr oxides and silicates was also proposed [9] and extended to Ti oxides and silicates [10]. The behaviour of Hf and Zr oxides at the interface with Si was investigated [7] through a hypothetical tetragonal Si-epitaxial crystalline phase obtained by imposing the in-plane lattice constant of Si and adjusting the axial ratio and internal coordinates. Finally, amorphous Zr silicates were analysed in detail [8] and a microscopic scheme that relates the dielectric constants to the local bonding of Si and Zr atoms was proposed. Very recently, group IIIb transition metal oxides have also been investigated from first principles [11, 12]. From a comparison between the cubic (bixbyite) and hexagonal forms of Lu_2O_3, it was suggested [11] that sesquioxides in the bixbyite structure (e.g. Y_2O_3 and Lu_2O_3) will consistently have dielectric constants smaller than those in the hexagonal structure (e.g. La_2O_3).

For completeness, it should be mentioned that a considerable amount of DFT studies has also been devoted to perovskite (ABO_3) transition metal oxides due to their interesting ferroelectric/antiferroelectric behaviour. These would deserve a complete topical review on their own and hence will not be presented here. Instead, a list of useful references [28] is provided for the interested reader. This list is far from being exhaustive: it mainly includes papers dealing with the dielectric properties of perovskites or presenting some recent state-of-the-art calculations.

In this topical review, a presentation is given of the contribution of density-functional theory to the study of the dielectric properties of crystalline and amorphous transition metal oxides and silicates considered as potential high-κ dielectrics. Section 2 is devoted to a presentation of the principal equations related to the dielectric properties. In section 3, the results obtained for various crystalline systems are discussed. For group IVb transition metals (M = Hf, Zr, Ti), the dielectric properties are compared between the cubic, tetragonal, monoclinic, and rutile phases of MO_2 oxides and the crystalline silicates $MSiO_4$. For group IIIb transition metals, the cubic (bixbyite) and hexagonal phases of Lu_2O_3 are discussed. Section 4 is dedicated to the study of amorphous silicates. For this purpose, a scheme recently introduced is discussed which relates the dielectric constants to the local bonding of silicon and transition metal atoms. The central idea is to define of characteristic parameters for the basic structural units (SUs) formed by Si and TM atoms and their nearest neighbours. With this scheme, heavy large-scale calculations, which are beyond current computational capabilities, are avoided. Applied to amorphous Zr silicates, this scheme provides a good description of the measured dielectric constants, both of the optical and the static ones. Finally, in section 5, conclusions are presented.

2. Theoretical background

In this brief overview, only the main equations related to the dielectric properties of materials will be presented. These are connected to the *responses* of solid systems to two types of perturbations: (a) collective displacements of atoms and (b) homogeneous static electric fields.

These responses can be obtained in the framework of DFT using various methods, which can be found in the nice review article by Baroni *et al* [29]. The equations presented hereafter have been implemented in the PWSCF [30] and ABINIT [31] packages which are both distributed under the GNU General Public Licence.

For insulators, the dielectric permittivity tensor is defined as the coefficient of proportionality between the macroscopic displacement field $\mathcal{D}_{\rm mac}$ and the macroscopic electric field $\mathcal{E}_{\rm mac}$, in the linear regime:

$$\mathcal{D}_{{\rm mac},\alpha} = \sum_{\beta} \epsilon_{\alpha\beta} \mathcal{E}_{{\rm mac},\beta}. \tag{1}$$

It can be obtained as

$$\epsilon_{\alpha\beta} = \frac{\partial \mathcal{D}_{{\rm mac},\alpha}}{\partial \mathcal{E}_{{\rm mac},\beta}} = \delta_{\alpha\beta} + 4\pi \frac{\partial \mathcal{P}_{{\rm mac},\alpha}}{\partial \mathcal{E}_{{\rm mac},\beta}}. \tag{2}$$

In general, the displacement $\mathcal{D}_{\rm mac}$, or the polarization $\mathcal{P}_{\rm mac}$, will include contributions from ionic displacements. In the presence of an applied field of high frequency, the contribution to the dielectric permittivity tensor resulting from the electronic polarization, usually noted $\epsilon^{\infty}_{\alpha\beta}$, dominates. This optical (ion-clamped) dielectric permittivity tensor is related to the second-order derivatives of the energy with respect to the macroscopic electric field [32].

At lower frequencies, supplementary contributions to the polarization coming from the ionic displacements must be included. In particular, at zero frequency, the static dielectric permittivity tensor, usually noted $\epsilon^{0}_{\alpha\beta}$, is obtained by

$$\epsilon^{0}_{\alpha\beta} = \epsilon^{\infty}_{\alpha\beta} + \sum_{m} \Delta\epsilon_{m,\alpha\beta} = \epsilon^{\infty}_{\alpha\beta} + 4\pi \sum_{m} \frac{f^{2}_{m,\alpha\beta}}{\omega^{2}_{m}}, \tag{3}$$

where ω_m are the phonon frequencies at the centre of the Brillouin zone (Γ point) and $f_{m,\alpha\beta}$ are the oscillator strength tensors[1].

The squares of the phonon frequencies ω^2_m at the Γ point are determined as eigenvalues of the dynamical matrix $\tilde{D}_{\kappa\alpha,\kappa'\beta}$, or as solutions of the following generalized eigenvalue problem:

$$\sum_{\kappa'\beta} \tilde{C}_{\kappa\alpha,\kappa'\beta} U_m(\kappa'\beta) = M_\kappa \omega^2_m U_m(\kappa\alpha), \tag{4}$$

where M_κ is the mass of the ion κ, and the matrix $\tilde{C}$ is related to the dynamical matrix $\tilde{D}$ through

$$\tilde{D}_{\kappa\alpha,\kappa'\beta} = \tilde{C}_{\kappa\alpha,\kappa'\beta} / \sqrt{M_\kappa M_{\kappa'}}. \tag{5}$$

The matrix $\tilde{C}_{\kappa\alpha,\kappa'\beta}$ is the Fourier transform of the matrix of the interatomic force constants. It is connected to the second-order derivatives of the total energy with respect to collective atomic displacements [32]. The eigenvectors $U_m(\kappa\alpha)$ are the atomic displacements for a given phonon mode m.

The oscillator strength tensors $f_{m,\alpha\beta}$ are defined as

$$f_{m,\alpha\beta} = \sqrt{\frac{1}{\Omega_0} \left(\sum_{\kappa\alpha'} Z_{\kappa,\alpha\alpha'} U^{*}_{m}(\kappa\alpha') \right) \left(\sum_{\kappa'\beta'} Z_{\kappa',\beta\beta'} U_m(\kappa'\beta') \right)}, \tag{6}$$

where Ω_0 is the volume of the primitive unit cell, and $Z_{\kappa,\beta\alpha}$ is the Born effective charge tensor. That is the proportionality coefficient relating, at linear order, the polarization per unit

[1] In the various papers that are summarized in this topical review, different definitions have been used for the oscillator strength tensors. For simplicity, a form compatible with all of them is adopted. This also presents the advantage that the oscillator strengths are expressed in the same units as the phonon frequencies.

cell, created along the direction β, and the displacement along the direction α of the atoms belonging to the sublattice κ, under the condition of zero electric field. The same coefficient also describes the linear relation between the force on an atom and the macroscopic electric field:

$$Z_{\kappa,\beta\alpha} = \Omega_0 \frac{\partial \mathcal{P}_{\mathrm{mac},\beta}}{\partial \tau_{\kappa\alpha}} = \frac{\partial F_{\kappa,\alpha}}{\partial \mathcal{E}_\beta}. \tag{7}$$

The Born effective charge tensors are connected to the mixed second-order derivative of the energy with respect to atomic displacements and macroscopic electric field [32].

The various DFT studies presented in this topical review have been performed using plane-wave basis sets. More technical details (program, pseudopotentials, energy cut-off, k-point sampling of the Brillouin zone) can be found in the appropriate references. Besides these works, some unpublished results (referred to as 'present work' in the tables 1–3 below) are also reported. These calculations have been performed using the ABINIT package [31, 33] with norm-conserving pseudopotentials [34, 35]. The wavefunctions are expanded in plane waves up to a kinetic energy cutoff of 30 Hartree. The Brillouin zone is sampled by a $4 \times 4 \times 6$ grid [36] is used that results in nine special k-points.

3. Crystalline systems

3.1. Introduction

The structural, electronic, dynamical, optical, and dielectric properties of group IIIb and IVb transition metal oxides and/or silicates have been the object of several first-principles studies [3–27]. This topical review focuses on the dielectric properties of these materials, which have been studied in [3–11] after a brief description of their structural properties.

On the one hand, the group IVb transition metals form dioxides (MO_2) which can adopt quite a variety of crystal structures: monoclinic, tetragonal, cubic, rutile, anatase, and brookite. Some of these group IVb TMs also appear in nature as crystalline silicates with the formula $MSiO_4$. The dielectric properties of quite a number of these crystalline structures have been investigated from first principles: monoclinic HfO_2 [6] and ZrO_2 [5]; tetragonal and cubic HfO_2 [6, 9], ZrO_2 [4, 5], and TiO_2 [10]; rutile TiO_2 [10]; and the silicates $HfSiO_4$ [10], $ZrSiO_4$ [3], and $TiSiO_4$ [10]. On the other hand, the group IIIb transition metals form sesquioxides (M_2O_3) which can have either the cubic (bixbyite) structure (e.g. Y_2O_3 and Lu_2O_3) or the hexagonal structure (e.g. La_2O_3). Using first-principles calculations, the dielectric properties of Lu_2O_3 have been studied for both the cubic phase and for a hypothetical hexagonal phase [11].

All the calculations reported in this topical review have been performed within the localized density approximation (LDA) to DFT theory [37, 38]. In the case of HfO_2, a comparison [6] has been made between the LDA and the generalized gradient approximation (GGA). The LDA and GGA results do not differ significantly for the structural and dielectric properties.

3.2. Group IVb transition metals

Titania (TiO_2) is by far the most important compound formed by the transition metals of group IVb, its importance arising predominantly from its use as a white pigment. Three forms exist at room temperature: rutile, anatase, and brookite. Each of them occurs naturally. Rutile is the most common form, both in nature and as produced commercially. It is also the most stable phase: the others transform into it on heating. Note also that all three forms contain sixfold coordinated titanium atoms. Hafnia (HfO_2) and zirconia (ZrO_2) undergo polymorphic

Table 1. Structural parameters for the cubic (c), tetragonal (t), monoclinic (m), and rutile (r) phases of group IVb transition metal M = (Hf, Zr, Ti) oxides MO_2 and for silicates $MSiO_4$: a comparison between theory and experiment. The lengths are expressed in Å.

		M = Hf		M = Zr		M = Ti	
		Th.	Expt.	Th.	Expt.	Th.	Expt.
c-MO_2		Ref. [9]	Ref. [43]	Ref. [4]	Ref. [42]	Ref. [10]	
	a	5.11	5.08	5.01	5.09	4.72	
t-MO_2		Ref. [9]	Ref. [43]	Ref. [4]	Ref. [42]	Ref. [10]	
	a	5.11	5.15	5.02	5.05	4.71	
	c	5.17	5.29	5.09	5.18	4.93	
	d_z	0.031	—	0.040	0.057	0.070	
m-MO_2		Ref. [6]	Ref. [44]	Ref. [5]	Ref. [42]		
	a	5.106	5.117	5.108	5.15		
	b	5.165	5.175	5.170	5.21		
	c	5.281	5.291	5.272	5.32		
	β	99.35	99.22	99.21	99.23		
	x_M	0.280	0.276	0.277	0.275		
	y_M	0.043	0.040	0.042	0.040		
	z_M	0.209	0.208	0.210	0.208		
	x_{O1}	0.076	0.074	0.069	0.070		
	y_{O1}	0.346	0.332	0.333	0.332		
	z_{O1}	0.337	0.347	0.345	0.345		
	x_{O2}	0.447	0.449	0.450	0.450		
	y_{O2}	0.759	0.758	0.757	0.756		
	z_{O2}	0.483	0.480	0.480	0.479		
r-MO_2		Present work		Present work		Ref. [10]	Ref. [45]
	a	4.90		4.80		4.53	4.59
	c	3.27		3.22		2.92	2.96
	u	0.305		0.305		0.303	0.304
$MSiO_4$		Ref. [9]	Ref. [46]	Ref. [3]	Ref. [47]	Ref. [10]	
	a	6.61	6.57	6.54	6.61	6.21	
	c	5.97	5.96	5.92	6.00	5.81	
	u	0.067	0.066	0.065	0.065	0.059	
	v	0.196	0.195	0.195	0.197	0.189	

transformations with changes in external parameters. At high temperature, the compounds are highly defective and their structure is fluorite type ($Fm\bar{3}m$). The decreasing temperature induces a cubic to tetragonal ($P4_2/nmc$) phase transition (c–t) at about 2650 °C for HfO_2 [39] and about 2350 °C for ZrO_2 [40]. This transition is followed by a tetragonal to monoclinic ($P2_1/c$) martensitic phase transition (t–m) at about 1650 °C for hafnia [41] and about 1150 °C for zirconia [42]. In the cubic and tetragonal phase, the metal atoms are eightfold coordinated while in the monoclinic phase they are sevenfold coordinated. None of the existing phases have sixfold coordinated atoms as in the rutile structure.

Hafnon ($HfSiO_4$) and zircon ($ZrSiO_4$) are the crystalline silicates of group IVb transition metals. They are both naturally occurring gemstones, often colourless. Zircon can also be yellow, orange, red, blue, brown and green. It resembles diamond in its lustre and fire (because

Table 2. Electronic (ϵ_∞) and static (ϵ_0) dielectric tensors for the cubic (c), tetragonal (t), monoclinic (m), and rutile (r) phases of group IVb transition metal M = (Hf, Zr, Ti) oxides MO_2 and for silicates $MSiO_4$ (for t-TiO_2, the static dielectric tensor cannot be calculated due to the instability of the phase; see the discussion in the text). The tensors are diagonal in all cases except for the monoclinic phase, in which it is only block diagonal in y and xz subspaces. For the cubic phase, the tensor is also isotropic. For the tetragonal and rutile phases of MO_2 as well as for $MSiO_4$, the tensors have different components parallel ($\parallel$) and perpendicular ($\perp$) to the c axis. The total lattice contribution ($\epsilon_{\text{latt.}}$) to ϵ_0 is also indicated.

		M = Hf			M = Zr			M = Ti		
		ϵ_∞	$\epsilon_{\text{latt.}}$	ϵ_0	ϵ_∞	$\epsilon_{\text{latt.}}$	ϵ_0	ϵ_∞	$\epsilon_{\text{latt.}}$	ϵ_0
c-MO_2		Ref. [9]			Ref. [4]			Ref. [10]		
		5.37	20.80	26.17	5.74	27.87	33.61	9.11	128.36	137.47
t-MO_2		Ref. [9]			Ref. [4]			Ref. [10]		
	$\parallel$	5.13	14.87	20.00	5.28	15.03	20.31	6.66	—	—
	$\perp$	5.39	27.42	32.81	5.74	42.39	48.13	8.81	—	—
m-MO_2		Ref. [6]			Ref. [5]					
	yy	—	10.75	—	—	15.56	—			
	xx	—	11.70	—	—	16.70	—			
	zz	—	7.53	—	—	13.12	—			
	xz	—	1.82	—	—	0.98	—			
r-MO_2		Present work			Present work			Ref. [10]		
	$\parallel$	5.19	19.39	24.58	5.54	26.27	31.81	8.57	116.17	124.74
	$\perp$	4.59	19.03	23.62	4.93	26.71	31.64	7.49	88.79	96.28
$MSiO_4$		From [9]			From [3]			From [10]		
	$\parallel$	4.11	6.54	10.65	4.26	7.27	11.53	5.52	11.21	16.73
	$\perp$	3.88	6.75	10.63	4.06	7.90	11.96	5.56	13.88	19.44

of its high refractive index), yet it has a tendency to chip out at the facet junctions over the years, so it is not prized as highly. Hafnon is isomorphous with zircon and often occurs together with it. Because of this resemblance, it is rarely identified separately when found, and therefore hafnon is hardly known to mineral collectors. In reality, it is much more prevalent than perceived. These two minerals are members of the orthosilicate group of great geological significance. Zircon and hafnon have also been widely investigated in the framework of the disposal of nuclear waste. Indeed, there are two other $MSiO_4$ crystalline silicates occurring in nature: thorite with M = Th and coffinite with M = U. Besides, $PuSiO_4$ has also been synthesized. All these $MSiO_4$ silicates exhibit the same crystalline structure, suggesting that extensive substitution of Zr or Hf by radioactive elements is possible in zircon and hafnon.

The cubic phase of the MO_2 oxides of group IVb transition metals M = (Hf, Zr, Ti) takes the fluorite structure (space group $Fm\bar{3}m$, No 225), which is fully characterized by a single lattice constant a. The M = (Hf, Zr, Ti) atoms are in a face-centred-cubic (FCC) structure, and the O atoms occupy the tetrahedral interstitial sites associated with this FCC lattice. The primitive unit cell contains one formula unit of MO_2 with M = (Hf, Zr, Ti), while the conventional unit cell has four of them, as represented in figure 1(a).

The tetragonal phase (space group $P4_2/nmc$, No 137) can be viewed as a distortion of the cubic structure obtained by displacing alternating pairs of O atoms up and down by an amount

Table 3. Frequencies (ω_m in cm^{-1}), oscillator strengths (f_m in cm^{-1}), and contributions to the dielectric constants ($\Delta\epsilon_m$) of the various IR modes for the cubic (c), tetragonal (t), monoclinic (m), and rutile (r) phases of HfO_2, ZrO_2, and TiO_2, and for $HfSiO_4$, $ZrSiO_4$, and $TiSiO_4$.

		M = Hf			M = Zr			M = Ti		
		ω_m	f_m	$\Delta\epsilon_m$	ω_m	f_m	$\Delta\epsilon_m$	ω_m	f_m	$\Delta\epsilon_m$
c-MO_2		Ref. [9]			Ref. [4]			Ref. [10]		
	F_{1u}	285	367	20.80	280	417	27.87	177	566	128.36
t-MO_2		Ref. [9]			Ref. [4]			Ref. [10]		
	A_{2u}	315	343	14.87	339	371	15.03	429	382	9.97
	E_u (1)	185	247	22.34	153	257	35.48	116i	284	—
	E_u (2)	428	272	5.08	449	333	6.91	496	522	13.94
m-MO_2		Ref. [6]			Ref. [5]					
	A_u (1)	140	8	0.04	181	11	0.05			
	A_u (2)	190	1	0.00	242	38	0.31			
	A_u (3)	255	129	3.21	253	145	4.10			
	A_u (4)	393	194	3.06	347	184	3.54			
	A_u (5)	445	206	2.68	401	264	5.44			
	A_u (6)	529	141	0.89	478	156	1.34			
	A_u (7)	661	133	0.51	571	141	0.77			
	A_u (8)	683	116	0.36	634	10	0.00			
	B_u (1)	246	149	4.60	224	141	4.97			
	B_u (2)	262	21	0.08	305	71	0.69			
	B_u (3)	354	273	7.47	319	289	10.33			
	B_u (4)	378	190	3.16	355	254	6.43			
	B_u (5)	449	253	3.98	414	214	3.37			
	B_u (6)	553	137	0.77	483	196	2.07			
	B_u (7)	779	169	0.59	711	149	0.55			
r-MO_2		Present work			Present work			Ref. [10]		
	A_{2u}	308	382	19.38	301	435	26.27	204	620	116.16
	E_u (1)	193	186	11.64	197	247	19.69	180	459	81.65
	E_u (2)	222	104	2.74	302	97	1.30	404	194	2.90
	E_u (3)	478	291	4.65	462	312	5.72	502	291	4.23
$MSiO_4$		From [9]			From [3]			From [10]		
	A_{2u} (1)	321	201	4.93	348	238	5.90	319	283	9.90
	A_{2u} (2)	598	152	0.81	601	122	0.52	606	95	0.31
	A_{2u} (3)	983	248	0.80	980	255	0.85	1000	284	1.01
	E_u (1)	252	149	4.38	285	183	5.16	303	290	11.54
	E_u (2)	395	96	0.75	383	124	1.31	374	0	0.00
	E_u (3)	420	70	0.35	422	27	0.05	433	83	0.46
	E_u (4)	873	278	1.27	867	287	1.38	877	339	1.88

Δz along the z direction, as marked by the arrows in figure 1(b), and by applying a tetragonal strain. The resulting primitive cell is doubled compared to the cubic phase, including two formula units of MO_2. The conventional unit cell, which is reproduced in figure 1(b), has four formula units of MO_2 with M = (Hf, Zr, Ti). The tetragonal structure is completely specified by two lattice constants (a and c) and the dimensionless ratio $d_z = \Delta z/c$ describing

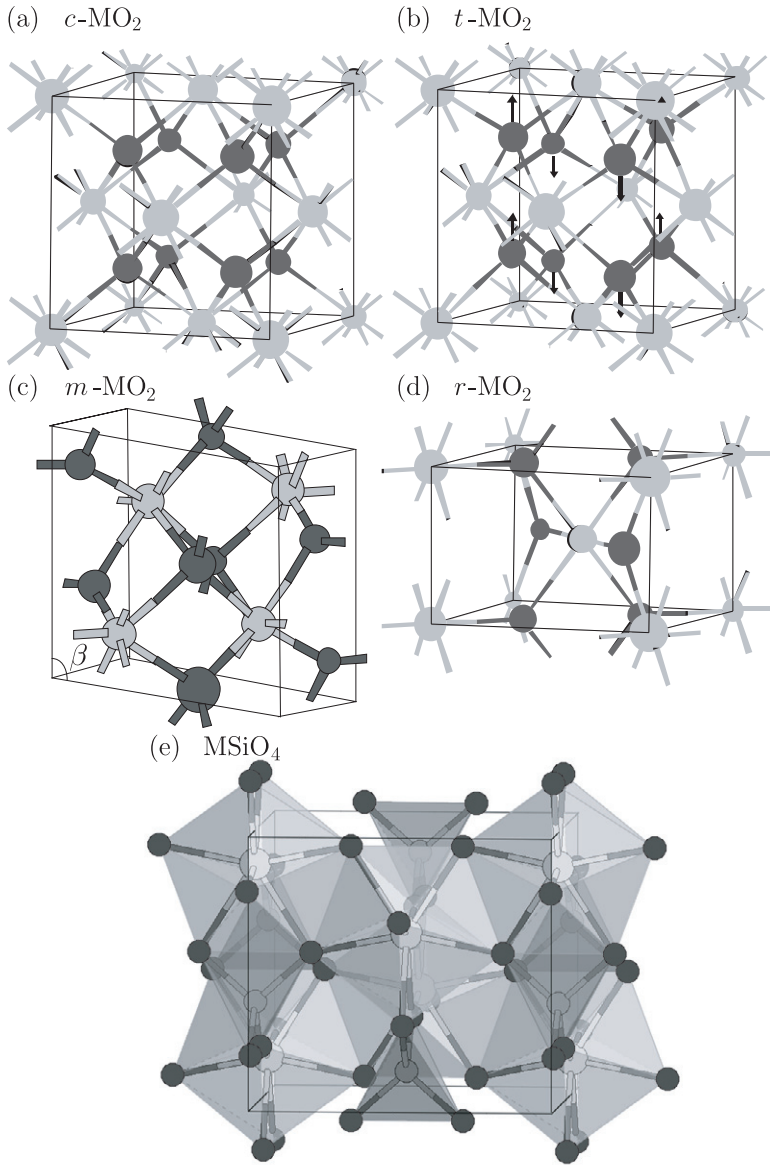

Figure 1. Structures of the (a) cubic, (b) tetragonal, (c) monoclinic, and (d) rutile phases of the MO_2 oxide, and of the silicate $MSiO_4$ for group IVb metals M = (Hf, Zr, Ti). A ball and stick representation is adopted where M = (Hf, Zr, Ti) and O atoms are coloured in light and medium grey, respectively. For the tetragonal phase of the MO_2 oxides, the arrows indicate the displacements of oxygen pairs relative to the cubic structure. For the silicate, the SiO_4 tetrahedra and MO_8 dodecahedra have also been represented.

the displacement of the O atoms. The cubic phase can be considered as a special case of the tetragonal structure with $d_z = 0$ and $c/a = 1$ (if the primitive cell is used for the tetragonal phase, $c/a = \sqrt{2}$).

The monoclinic phase has a lower symmetry (space group $P2_1/c$, No 14) and a more complex geometric structure with 12 atoms in the primitive cell. The lattice parameters are

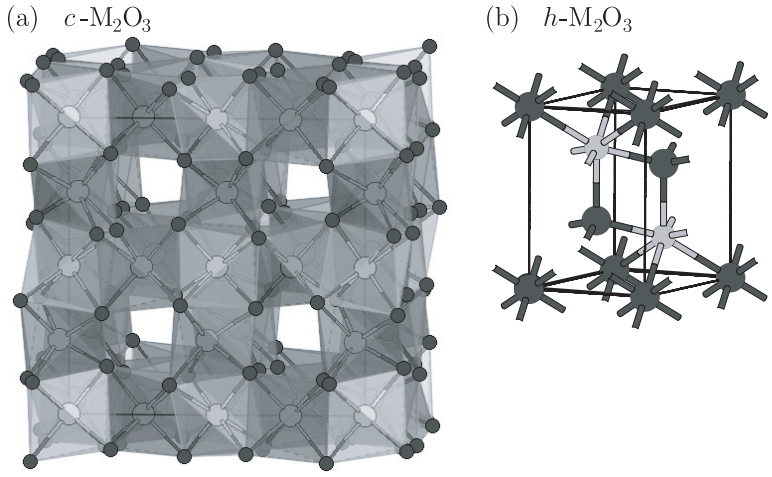

Figure 2. Structures of the (a) cubic (bixbyite) and (b) hexagonal phases of the M_2O_3 oxide for group IIIb metals M = (Y, La, Lu). A ball and stick representation is adopted where M = (Y, La, Lu) and O atoms are coloured in light and medium grey, respectively. For the cubic phase, the M1 atoms are coloured with a lighter grey than the M2 atoms and the octahedra centred on these atoms have also been represented with the same colour scheme.

a, b, c, and β (the non-orthogonal angle between a and c) as shown in figure 1(c). All the atoms occupy 4e Wyckoff sites (x, y, z) with parameters x, y, and z specified for M atoms and two non-equivalent oxygen atoms O1 and O2. Note that the atoms of type O1 are threefold coordinated, while O2 are fourfold coordinated. All M atoms are equivalent and are sevenfold coordinated. Four lattice-vector parameters and nine internal parameters are needed to fully specify the structure.

The rutile structure (space group $P4_2/mnm$, No 136) has a tetragonal unit cell with two formula units of MO_2 with M = (Hf, Zr, Ti). The metal atoms occupy the body-centred-cubic positions (2a Wyckoff sites) and the O atoms are at the 4f Wyckoff sites (u, u, 0), as reported in figure 2(c). The rutile structure is completely specified by two lattice constants (a and c) and the internal parameter u related to the position of O atoms.

The $MSiO_4$ with M = (Hf, Zr, Ti) crystal has a conventional unit cell which is body-centred tetragonal (space group $I4_1/amd$, No 141) and contains four formula units of $MSiO_4$. A primitive cell containing only two formula units of $MSiO_4$ can also be defined. The $MSiO_4$ crystal consists of alternating (discrete) SiO_4 tetrahedra and MO_8 dodecahedra, sharing edges to form chains parallel to the c direction, as illustrated in figure 1(e). Note that in the MO_8 dodecahedra four O atoms are closer to the M atom than the four other ones. The positions of the M = (Hf, Zr, Ti) and Si atoms are imposed by symmetry: they are located at (0, $\frac{3}{4}$, $\frac{1}{8}$) and (0, $\frac{1}{4}$, $\frac{3}{8}$) on the 4a and 4b Wyckoff sites respectively. The O atoms occupy the 16h Wyckoff sites (0, u, v), where u and v are internal parameters.

The calculated structural parameters for the cubic, tetragonal, monoclinic, and rutile phases of group IVb transition metal M = (Hf, Zr, Ti) oxides MO_2, and for the silicates $MSiO_4$ are reported in table 1. For the naturally occurring phases, the available experimental values have also been indicated. The agreement is very good: the errors on the lattice constants are smaller than 2%, as is typical for LDA calculations. The structural parameters for Hf- and Zr-based oxides and silicates are very close, whereas those for Ti-based materials can be 5–10% closer. It is interesting to take a closer look at this observation.

Considering the valence electrons only, the electron configurations of Hf, Zr, and Ti differ only by the principal number of the occupied orbitals: it is $5d^26s^2$ for hafnium, $4d^25s^2$ for zirconium, and $3d^24s^2$ for titanium. Thus, in principle, they should be characterized by decreasing electronegativities and increasing atomic and ionic radii from Ti to Hf. However, in the periodic table, the inner transition (rare-earth) elements immediately preceding Hf add electrons to the inner 4f shell from element No 58, cerium, to No 71, lutetium (it would actually be more correct to write that the electron configuration of hafnium is $4f^{14}5d^26s^2$). Because the nuclear charge increases while no additional outer shells are filled, there is a contraction in the atomic size. Consequently, element No 72, hafnium, has a slightly smaller atomic size than element No 40, zirconium, the group IVb element in the preceding row. This results in the so-called lanthanide contraction.

As a consequence, while the atomic radius of Ti (1.40 Å) is indeed smaller than for Zr (1.55 Å), the atomic radius of Hf (1.55 Å) is identical to that of Zr [48]. The ionic radii (M^{4+}) also present the same anomaly: it is smaller for Ti (0.61 Å) than for Zr (0.84 Å), but it is essentially the same for the latter and Hf (0.84 Å) [49]. Finally, their electronegativities also show an anomalous trend with values of 1.23 for hafnium and 1.22 for zirconium, compared to 1.32 for Ti [50]. All this explains the origin of the close similarity between Hf and Zr oxides and silicates with respect to Ti ones.

Turning to the calculations of the dielectric properties of these crystalline systems, the electronic (ϵ_∞) and static (ϵ_0) permittivity tensors are diagonal and isotropic in the cubic phase. Due to the tetragonal symmetry of t-MO_2, r-MO_2, and $MSiO_4$ crystals, these tensors are also diagonal for these phases, but they have two independent components $\epsilon_\parallel$ and $\epsilon_\perp$, parallel and perpendicular to the c axis, respectively. For the m-MO_2, the permittivity tensors are only block diagonal in y and xz subspaces. Hence, they have four independent components ϵ_{yy}, ϵ_{xx}, ϵ_{zz}, and ϵ_{xz}. In table 2, the calculated values of ϵ_∞ and ϵ_0 [3–6, 9, 10] are reported for the cubic, tetragonal, monoclinic, and rutile phases of hafnia, zirconia, and titania, as well as for hafnon, zircon, and titanon. The total lattice contribution ($\epsilon_{\text{latt.}} = \epsilon_0 - \epsilon_\infty$) is also presented.

In the tetragonal phase, the ϵ_∞ tensor is only slightly anisotropic with about 5% and 10% difference between the parallel and perpendicular values for hafnia and zirconia. For titania, it is a bit more anisotropic with about 25% difference between these values. In contrast, the ϵ_0 tensor is highly anisotropic: the value of ϵ_0 in the direction parallel to the c axis is 1.6 and 2.4 times smaller than that in the perpendicular direction for t-HfO_2 and t-ZrO_2, respectively. For t-TiO_2, the static dielectric tensor cannot be calculated due to the instability of the phase (the E_u mode with an imaginary frequency tends to break the symmetry imposed in the calculation).

For the monoclinic phase, the optical and static dielectric permittivities have not been calculated explicitly in [5, 6]. But, it is clear that $\epsilon_{\text{latt.}}$ will definitely contribute to the anisotropy of the ϵ_0 tensor. The ratio between the largest and the smallest increments with respect to the ϵ_∞ tensor, which are found in the xz plane, is roughly 1.5 and 2 for m-HfO_2 and m-ZrO_2, respectively.

In the rutile phase, the ϵ_∞ tensors present the same relatively small difference (12%) between $\epsilon_\parallel$ and $\epsilon_\perp$ for the three oxides. For hafnia and zirconia, the anisotropic character is reduced for the static dielectric permittivity tensor with 4% and 1% difference between its parallel and perpendicular components, respectively. For titania, ϵ_0 is more anisotropic than ϵ_∞.

The calculated dielectric tensors can only be compared with experimental values for the naturally occurring phases (i.e. the cubic, tetragonal, and monoclinic phases of hafnia and zirconia, for the rutile phase of titania, and for zircon)[2]. Moreover, a direct comparison is

[2] For hafnon, no accurate measurements could be found in the literature.

very difficult since there are very few data available in the literature, especially for hafnia. The main problem encountered in the experimental determination of the dielectric properties is that good quality single crystals are not available.

For the tetragonal and monoclinic phases, the experimental results have been obtained on polycrystalline samples and must be analysed in the framework of effective medium theory [51]. As a result, a unique value of ϵ is found without distinction between the various preferential directions (parallel and perpendicular to the c axis for the tetragonal phase, along the y direction and in the xz plane for the monoclinic phase). In order to compare these results with experimental data, an orientational average must be taken.

For hafnia, only measurements of ϵ_0 are reported in the literature. The calculated values of 26.17 for the cubic phase, $\bar{\epsilon}_0 = 28.54$ for the tetragonal phase, and $\bar{\epsilon}_0 = 15.47$ for the monoclinic phase[3] agree reasonably well with the values of 16 [52] and 20 [53] obtained in recent measurements on thin films.

For zirconia, an experimental value of $\epsilon_\infty = 4.8$ is reported in the literature for c-ZrO_2 [54, 55], while measured values for t-ZrO_2 range between 4.2 [56] and 4.9 [57]. The theoretical values ($\epsilon_\infty = 5.74$ and $\bar{\epsilon}_\infty = 5.59$ for the cubic and tetragonal phases, respectively) are larger than the experimental ones by about 10–15%, as often found in the LDA to DFT. For ϵ_0, the experimental values found in the literature vary from 27.2 [58] to 29.3 [59] for c-ZrO_2, from 34.5 [58] to 39.8 [59] for t-ZrO_2, and from 12.5 [60] and 17.0 [61]. For the cubic and the monoclinic phases, the calculated values $\epsilon_0 = 33.61$ and $\bar{\epsilon}_0 = 19.65$ are slightly larger than experimental estimates, whereas for the tetragonal phase, the calculated average $\bar{\epsilon}_0 = 38.86$ falls in the range of the experimental data.

For titania, the experimental values of the electronic permittivity tensor for the rutile phase are 6.84 and 8.43 in the directions perpendicular and parallel to the c axis [62]. The corresponding theoretical values of 7.49 and 8.57 also present the usual 10% overestimation of the LDA. For the static dielectric permittivity tensor, the theoretical values are of the same order of magnitude as the experimental results, which show quite large discrepancies: from 86 and 170 [63] to 115 and 251 [64] for the components perpendicular and parallel to the c axis, respectively.

For zircon, values of 10.69(3.8) [65] and 11.25(3.5) [66] are reported for the static (electronic) dielectric permittivity in the directions parallel and perpendicular to the tetragonal axis, respectively. The theoretical values overestimate of the experimental results by about 10%, as typically observed in LDA. For hafnon, the only possible comparison is with amorphous hafnium silicates, for which values ranging from 11 to 25 have been reported.

For a deeper analysis, the static dielectric tensor can be decomposed in the contributions of different modes as indicated in equation (3). Such an analysis reveals the importance of the frequencies of the IR-active modes and their oscillator strengths.

The contributions of each IR-active mode $\Delta\epsilon_m$ to the static dielectric constants are presented in table 3 for all the crystalline oxides and silicates discussed above (except for the t-TiO_2 phase), together with the corresponding frequencies and oscillator strength tensors. The latter is isotropic for the F_{1u} mode in the cubic phase. In the tetragonal and rutile phases as well as in the crystalline silicates $MSiO_4$, f_m refers to the parallel–parallel component for the A_{2u} mode, and to the perpendicular–perpendicular component for the E_u modes. In the monoclinic phase, the A_u modes produce contributions to the yy component of the static dielectric tensor while the B_u modes contribute to the three components in the xz plane.

[3] As mentioned above, the optical dielectric tensor for the monoclinic phase has not been computed in [5, 6]. For the purposes of comparison with the static dielectric responses, the authors have arbitrarily assumed an isotropic value of $\bar{\epsilon}_\infty = 5.0$.

In table 3, the lowest frequency modes provide the largest contributions to ϵ_0 (except for the monoclinic phase which does not show a clear trend and will be omitted in the following discussion), even if their oscillator strength (f_m) is relatively small. For instance, the $E_u(1)$ mode in the tetragonal and rutile phases of hafnia and zirconia contributes much more to the static dielectric permittivity than the $E_u(2)$ mode in the tetragonal phase and the $E_u(3)$ mode in the rutile phase, which present however larger values of f_m. This emphasizes the crucial role of the frequency factor in equation (3). That is particularly true for the cubic phase for TiO_2 compared to ZrO_2 and HfO_2. In this case, the frequency of the F_{1u} mode in titanium oxide is more than 35% smaller than in the other two oxides. This reduced frequency as well as the increased oscillator strength (see the discussion in [10]) leads to a static dielectric constant more than four times larger in c-TiO_2.

In the tetragonal phase of hafnia and zirconia, the same argument holds to rationalize why the ϵ_0 tensor is highly anisotropic, while the ϵ_∞ tensor is only slightly anisotropic. Indeed, in these materials, the A_{2u} has the largest oscillator strength (about twice that of $E_u(1)$ mode) and the largest mode-effective charge. However, its frequency is about twice as large as that of the $E_u(1)$ mode, and its contribution to the static dielectric constant is thus roughly twice as small as that of the $E_u(1)$ mode.

In table 3, it can be observed that the oscillator strengths essentially increase from HfO_2 to ZrO_2 and from ZrO_2 to TiO_2, and the same trend holds for the silicates. This can be related [9, 10] to the behaviour of the Born effective charges $Z_{\kappa,\alpha\alpha'}$ and the eigendisplacements $U_m(\kappa\alpha)$, the two quantities that appear in the definitions of $f_{m,\alpha\beta}$ given in equation (6). On the one hand, the Born effective charges show globally the following trend: $Z(HfO_2) \leqslant Z(ZrO_2) \leqslant Z(TiO_2)$ and $Z(HfOSi_4) \leqslant Z(ZrSiO_4) \leqslant Z(TiSiO_4)$. On the other hand, the displacements of Hf atoms are smaller than those of Zr atoms, which in turn are smaller than those of Ti atoms, simply because the mass increases from Ti to Hf (as discussed in [9, 10]).

If one now considers the contributions to the static dielectric constant reported in table 3, it appears clearly that $\Delta\epsilon(HfO_2) \leqslant \Delta\epsilon(ZrO_2) \leqslant \Delta\epsilon(TiO_2)$ for almost of all the modes, following the increasing trend of the oscillator strengths discussed above. For a few modes, however, despite the increasing trend for f_m, the corresponding contribution presents exactly the opposite trend due to an increase of the corresponding phonon frequencies. For instance, for the $E_u(3)$ mode in the rutile phase, the frequency for ZrO_2 is much smaller than for TiO_2. As a result, the increase by 220% of the oscillator strengths is completely compensated by the rise of 34% in the frequency: in the end, the contribution for TiO_2 is 9% larger than the one for ZrO_2. For the crystalline silicates, the phonon frequencies do not change significantly from Hf to Zr and from Zr to Ti, and consequently the increasing trend in the oscillator strengths essentially dominates and $\Delta\epsilon(HfSiO_4) \leqslant \Delta\epsilon(ZrSiO_4) \leqslant \Delta\epsilon(TiSiO_4)$ (see, in particular, the lowest and highest frequency modes).

In the crystals with tetragonal symmetry (t-MO_2, r-MO_2, and $MSiO_4$), the lowest and highest frequency modes for each symmetry representation (A_{2u} and E_u) exhibit the largest oscillator strengths. Despite their similar f_m, the modes of lowest frequency contribute much more to the static dielectric constant than the modes of highest frequency, the frequency factor in equation (3) playing a crucial role. The other modes contribute significantly less to the static dielectric constants.

3.3. Group IIIb transition metals

The sesquioxides M_2O_3 of group IIIb transition metals are white solids which can be prepared directly from the elements. Yttria (Y_2O_3) is one of the most important sesquioxides within the general class of refractory ceramics. Y_2O_3 has many applications such as sintering aids in the

Table 4. Calculated structural parameters for the cubic (c) and hexagonal (h) phases of Lu_2O_3 oxide (from [11]). The lengths are expressed in Å.

c-Lu_2O_3		h-Lu_2O_3	
a	10.39	a	3.63
u	0.032	u	0.248
x	0.391	v	0.648
y	0.152		
z	0.379		

processing of ceramic materials, substrates for semiconducting films, optical windows, and components for rare-earth doped lasers. Lutetia (Lu_2O_3) is an important raw material for laser crystals. It has specialized uses in ceramics, glass, phosphors, and lasers. It can also be used as catalysts in cracking, alkylation, hydrogenation, and polymerization. Lanthana (La_2O_3) is widely used for very high transparency and refractive index in glass manufacturing industry. It is also used in x-ray image intensifying screens, phosphors, dielectric ceramics, conductive ceramics, and barium titanate capacitors.

In Y_2O_3 and Lu_2O_3, the metal atoms are sixfold coordinated. However, the larger La ion prefers to be sevenfold coordinated. Therefore, these oxides adopt two different crystalline structures: Y_2O_3 and Lu_2O_3 take a cubic structure, whereas La_2O_3 is hexagonal.

The cubic phase (space group $Ia3$, No 206) of the M_2O_3 oxides of the group IIIb transition metal is sketched in figure 2(a). The unit cell contains two inequivalent cation sites, M1 at the 8a Wyckoff site (0, 0, 0) and M2 at the 24d site (u, 0, $\frac{1}{4}$), and one type of O at the 48e site (x, y, z). The cubic cell contains a total of 80 atoms. The fluorite-like structure, named after the mineral bixbyite, can best be viewed as consisting of 64 slightly distorted mini-cubes with M = (Y, La, Lu) atoms sitting at the centres of 32 of the mini-cubes. The O atoms are at six of the eight corners of the cube such that an approximate octahedral coordination for the cation is maintained. The missing O are either at the face diagonal (75%) or at the end of the body diagonal (25%) of the mini-cube. For mini-cubes having M1 at the centre, three O are at one face of the cube, and the other three O are at the opposite face. The six M1–O bonds are equal in length. For mini-cubes containing M2, four O are at one face and the other two at the opposite face. There are three different pairs of M2–O bonds in terms of their length. On average, the M1–O bonds are slightly shorter than the M2–O bonds. Each O atom is linked to one M1 and three M2 atoms in the form of a distorted tetrahedron.

The hexagonal phase (space group $P\bar{3}m1$, No 164) is represented in figure 2(b). The unit contains two M cations at the 2d Wyckoff positions ($\frac{1}{3}$, $\frac{2}{3}$, u), and three oxygen atoms. Two of these oxygens occupy the same 2d positions with coordinates ($\frac{1}{3}$, $\frac{2}{3}$, v), and the remaining one is located at the position of the 1a site (0, 0, 0).

So far, the dielectric properties of group IIIb transition metal oxides have only been calculated for M = Lu [11]. Therefore, the focus will be on this material in what follows. The calculated structural parameters for the cubic and hexagonal phases of Lu_2O_3 oxide are reported in table 4. For the naturally occurring cubic phase, the calculated lattice constant is in excellent agreement with the experimental value of 10.39 [67].

Moving to the calculations of the dielectric properties of these two crystalline systems, the electronic (ϵ_∞) and static (ϵ_0) permittivity tensors are diagonal and isotropic in c-Lu_2O_3. Due to the symmetry of h-Lu_2O_3, these tensors are also diagonal for these phases, but they present two independent components $\epsilon_\parallel$ and $\epsilon_\perp$, parallel and perpendicular to the hexagonal axis, respectively. In table 5, the calculated values of ϵ_∞ and ϵ_0 [11] are reported for both the naturally occurring cubic and the hypothetical hexagonal phases.

Table 5. Electronic (ϵ_∞) and static (ϵ_0) dielectric tensors for the cubic (c) and hexagonal (h) phases of Lu_2O_3. In both cases, the tensors are diagonal. For the cubic phase, it is also isotropic, while for the hexagonal phase, the tensors have different components parallel ($\|$) and perpendicular ($\perp$) to the c axis. The total lattice contribution (ϵ_{latt}) to ϵ_0 is also indicated.

c-Lu_2O_3				h-Lu_2O_3		
ϵ_∞	$\epsilon_{\text{latt.}}$	ϵ_0		ϵ_∞	$\epsilon_{\text{latt.}}$	ϵ_0
4.18	7.80	11.98	$\|$	4.56	12.62	17.18
			$\perp$	4.65	14.69	19.34

Table 6. Frequencies (ω_m in cm^{-1}), oscillator strengths (f_m in cm^{-1}), and contributions to the dielectric constants ($\Delta\epsilon_m$) of the various IR modes for the cubic (c) and hexagonal (h) phases of Lu_2O_3.

c-Lu_2O_3				h-Lu_2O_3			
	ω_m	f_m	$\Delta\epsilon_m$		ω_m	f_m	$\Delta\epsilon_m$
$T_u(1)$	86	5	0.04	$A_{2u}(1)$	261	259	12.34
$T_u(2)$	114	1	0.00	$A_{2u}(2)$	497	74	0.28
$T_u(3)$	126	8	0.05	$E_u(1)$	221	225	13.00
$T_u(4)$	132	10	0.07	$E_u(2)$	494	182	1.70
$T_u(5)$	146	2	0.00				
$T_u(6)$	183	9	0.03				
$T_u(7)$	218	3	0.00				
$T_u(8)$	300	175	4.28				
$T_u(9)$	339	70	0.53				
$T_u(10)$	354	82	0.67				
$T_u(11)$	374	18	0.03				
$T_u(12)$	391	146	1.74				
$T_u(13)$	429	47	0.15				
$T_u(14)$	499	39	0.08				
$T_u(15)$	526	6	0.00				
$T_u(16)$	578	61	0.14				

As already discussed for group IVb transition metal oxides and silicates (see section 3.2), the contributions $\Delta\epsilon_m$ to the static dielectric constants can be analysed for each IR-active mode individually, based on equation (3). These contributions are presented in table 6, together with the corresponding frequencies and oscillator strength tensors. The latter is isotropic for the T_u mode in the cubic phase. In the hexagonal phase, f_m refers to the parallel–parallel component for the A_{2u} modes, and to the perpendicular–perpendicular component for the E_u modes.

For the cubic phase, the main contributions arise from the $T_u(8)$ and $T_u(12)$ IR modes at 300 and 391 cm^{-1}. Again, despite their similar oscillator strengths, the $T_u(8)$ mode contributes more than twice as much to ϵ_0 as the $T_u(12)$ mode due to its lower frequency. Many more IR active modes exist at low frequency, but their oscillator strengths are very low. The low-frequency modes involve cationic as well as anionic motion, and their pattern is very inefficient at producing dipole moments [11], whereas the intense IR modes around 300–400 cm^{-1} are predominantly (up to 80% of f_m) due to oxygen atomic displacements.

For the hexagonal phase, the largest contributions arise from the lowest frequency A_{2u} and E_u modes. These two modes show a very close ratio between f_m and ω_m, therefore their contributions to the static dielectric constant are very similar (5% difference). In contrast, the highest frequency A_{2u} and E_u modes have very different contributions to ϵ_0: their frequencies are practically identical, but their oscillator strengths differ by a factor 2.5. Hence, despite the

almost perfectly isotropic optical dielectric permittivity tensor, the resulting static dielectric permittivity tensor shows a bit more than 10% difference between the parallel and perpendicular components. The large oscillator strength of $A_{2u}(1)$ and $E_u(1)$ modes largely originates from oxygen-only atomic displacements [11].

The orientational average for the ϵ_0 value in the hexagonal phase is 18.62, which is more than a factor of 1.5 larger than the ϵ_0 value in the cubic phase. As the main difference in the dielectric constant between the cubic and hexagonal phases is due to the frequency and the oscillator strength of the oxygen-related IR modes, it has been suggested [11] that the preferred structure for the M_2O_3 sesquioxide determines the intensity of the dielectric screening. Therefore, disregarding possible additional differences in the Born effective charges, the hexagonal sesquioxides (e.g. La_2O_3) present a larger dielectric constant than the cubic ones (e.g. Y_2O_3), quite independently of the cation (Y or La). On this basis, the dielectric constants can be extrapolated to 10–15 for the cubic phases against 20–25 for the hexagonal ones [11].

4. Amorphous systems

The dielectric properties of transition metal amorphous silicates constitute an issue of great practical importance. Early experimental measurements tend to show a supra-linear dependence of the static dielectric constant ϵ_0 on the metal concentration [68, 69]. While several phenomenological theories address this behaviour [70, 71], a close to linear dependence seem to prevail based on more recent experimental findings [72, 73].

Addressing this technological issue using DFT calculations requires us to solve the more general problem of predicting the dielectric properties of amorphous alloys. Indeed, a brute force investigation of numerous large supercells is beyond present computational capabilities. A scheme to overcome this difficulty has recently been proposed in the case of amorphous Zr silicates [8]. In this topical review, the basic ideas of this scheme are described. The results of Rignanese *et al* [8] for Zr silicates are discussed and extended to the cases of Hf and Ti silicates. As a conclusion, a brief comparison between these different systems is given.

The scheme of Rignanese *et al* [8] is based on the definition of three parameters characteristic of the basic structural units (SUs) formed by Si and Zr atoms and their nearest neighbours: the electronic polarizability α_i, the dynamical charge Z_i, and the force constant C_i. The values of these parameters are obtained based on DFT calculations of the optical and static dielectric constants[4] for a series of crystal structures (nine models are considered in the study of Rignanese *et al* [8]).

From the optical dielectric constant (ϵ_∞), the characteristic electronic polarizability $\bar{\alpha}$ of each crystal structure can be determined using the Clausius–Mosotti relation [71, 73]:

$$\frac{\epsilon_\infty - 1}{\epsilon_\infty + 2} = \frac{4\pi}{3}\frac{\bar{\alpha}}{\bar{V}}, \tag{8}$$

where $\bar{V}$ is the average SU volume. The polarizability $\bar{\alpha}$ can be considered as a local and additive quantity, in contrast with ϵ_∞. Hence, the α_i values are defined for each SU i, where $i \equiv SiO_n$ (with $n = 4$ or 6) or ZrO_n (with $n = 4$, 6, or 8), in such a way that

$$\bar{\alpha} = \sum_i x_i \alpha_i, \tag{9}$$

where x_i is the molecular fraction. The actual α_i values are determined by solving in a least square sense the over-determined system based on the calculations of ϵ_∞ for the series of

[4] Orientational averages of ϵ_∞ and ϵ_0 are actually used.

Table 7. Polarizability (α in bohr^3), characteristic dynamical charge (Z), and characteristic force constant (C in Hartree/bohr^2) for various structural units, extracted from first-principles calculations for a series of nine crystalline models [8].

	SiO_4	SiO_6	ZrO_4	ZrO_6	ZrO_8
α	19.68	16.14	37.37	35.35	32.69
Z	4.29	4.92	5.66	7.16	6.73
C	0.3597	0.2176	0.4202	0.0817	0.1153

crystalline models. It was shown [8] that the values of ϵ_∞ derived from equations (8) and (9) using these α_i values are in very good agreement with those computed from first principles, presenting average and maximal errors smaller than 1% and 2.5%, respectively. It was also checked for an amorphous model that the value of $\epsilon_\infty = 3.25$ calculated with equations (8) and (9) compares very well with the first-principles result $\epsilon_\infty = 3.24$. These verifications give an *a posteriori* motivation for the use of equations (8) and (9) to model the optical dielectric constant.

From the difference ($\Delta\epsilon$) the static dielectric constant (ϵ_0) and the optical dielectric constant, the characteristic dynamical charge $\bar{Z}$ and characteristic force constant $\bar{C}$ of each crystal structure can be defined:

$$\Delta\epsilon = \epsilon_0 - \epsilon_\infty = 4\pi \sum_m \frac{f_m^2}{\omega_m^2} = \frac{4\pi}{\bar{V}} \frac{\bar{Z}^2}{\bar{C}}, \tag{10}$$

with

$$\bar{Z}^2 = \frac{1}{\bar{N}} \sum_\kappa Z_\kappa^2 \qquad \text{and} \qquad \bar{C}^{-1} = \bar{V} \sum_m \frac{f_m^2}{\omega_m^2 \bar{Z}^2}, \tag{11}$$

where Z_κ are the atomic Born effective charges, ω_m and f_m are the frequency and the oscillator strength of the mth mode, and the volume of the primitive unit cell Ω_0 is related to the volume $\bar{V}$ and to the number of SUs $\bar{N}$ by $\Omega_0 = \bar{N}\bar{V}$.

By analogy with the polarizability, Z_i and C_i values are defined for each SU such that

$$\bar{Z}^2 = \sum_i x_i Z_i^2 \qquad \text{and} \qquad \bar{C}^{-1} = \sum_i x_i C_i^{-1}, \tag{12}$$

though the locality and the additivity of these parameters is not guaranteed *a priori*. The optimal values Z_i and C_i are determined in the same way as for α_i.

It was shown [8] that, for the series of crystalline models, the values of $\Delta\epsilon$ obtained by introducing the parameters Z_i and C_i in equations (10) and (12) match quite well those calculated from first principles, though the agreement is not as impressive as for ϵ_∞. Differences result primarily from the determination of $\bar{C}$. By contrast, the values of $\bar{Z}$ given by equation (12) agree very well with those computed from first principles, showing an average and maximal error smaller than 2% and 3%, respectively. *A posteriori*, $\bar{C}$ appears to be less local and additive. In fact, it can be demonstrated that the locality of $\bar{C}$ is closely related to the dynamical charge neutrality of the SUs [8].

For the amorphous model, which was not used to determine the Z_i and C_i values, the agreement between the model and the first-principles $\Delta\epsilon$ is excellent, with an error smaller than 1% [8]. Indeed, the scheme is more accurate for disordered systems, where the localization of vibrational modes is enhanced and the dynamical charge neutrality appears better respected.

The parameters α_i, Z_i, and C_i, reported in table 7 for the case of Zr silicates [8], fully determine the dielectric constants of an amorphous system of known composition in terms of SUs. It is important to note the following two points. On the one hand, the three

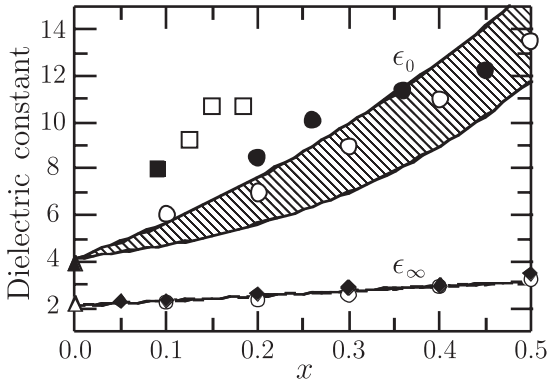

Figure 3. Dielectric constants (ϵ_∞ and ϵ_0) as a function of composition x for amorphous $(ZrO_2)_x(SiO_2)_{1-x}$. The hatched region corresponds to results derived from the model scheme and reflects the indetermination of the number of ZrO_6 units. The upper curve delimiting the band corresponds to structures entirely composed of ZrO_6 units, while the lower curve represents a smooth transition from a structure composed of ZrO_4 units at $x = 0$ to one composed of ZrO_8 units at $x = 0.5$, without the occurrence of any ZrO_6 unit. The references for the experimental data are: ♦ [74], ● [72], ○ [73], □ [68, 69], ■ [75], ▲ [76], and △ [49].

parameters of Zr-centred SUs all contribute to enhancing the dielectric constants over those of Si-centred ones of corresponding coordination[5]. This is clearly at the origin of the increase of ϵ_∞ and ϵ_0 with increasing Zr concentration. Second, while the polarizability α_i of a given SU (Si- or Zr-centred) steadily decreases with increasing coordination, such a regular behaviour is not observed for the parameters Z_i and C_i determining $\Delta\epsilon$. On the other hand, Z_i and C_i concurrently vary to enhance the contribution of ZrO_6 units, which are the SUs giving the largest contribution to $\Delta\epsilon$ in amorphous Zr silicates.

Using the scheme given by equations (8)–(10) and (12), it is now possible to estimate ϵ_∞ and ϵ_0 for amorphous $(ZrO_2)_x(SiO_2)_{1-x}$ as a function of Zr composition ($0 < x < 0.5$). Using measured densities for Zr silicates [74], ϵ_∞ can be easily calculated as a function of x [8]. In this case, the effect of Zr coordination is negligible since the various Zr-centred units have close α values compared to SiO_4 (table 7). As plotted in figure 3, the theoretical values [8] agree very well with available experimental data [73, 74].

In order to apply the scheme for $\Delta\epsilon$, additional information on the cationic coordination is required. The Si atoms are assumed to be fourfold coordinated [8]. The coordination of Zr atoms is less well determined. Recent EXAFS measurements [70] tend to show that the average Zr coordination increases from about four to about eight for Zr concentrations increasing from $x \sim 0$ to $x \sim 0.5$. In figure 3, the calculated ϵ_0 for amorphous $(ZrO_2)_x(SiO_2)_{1-x}$ as a function of x [8] is plotted together with the available experimental data [68, 69, 72, 73, 75].

The characteristic parameters used to calculate ϵ_0 change noticeably with the local environment of Zr atoms. Therefore, the indetermination with respect to their coordination leads to a range of possible values for the theoretical values as represented by the dashed band in figure 3. Several suitable distributions of three representative structural units (ZrO_4, ZrO_6, and ZrO_8) have been considered [8]. The upper curve delimiting the band in figure 3 corresponds to structures entirely composed of ZrO_6 units. The lower curve is for amorphous systems which do not contain any ZrO_6 units. The average Zr coordination varies linearly from

[5] In table 7, the value of C for SiO_4 apparently leads to a higher contribution to $\Delta\epsilon$ than that for ZrO_4. This is an artefact of the approach used to determine the Z_i and C_i.

Table 8. Polarizability (α in bohr^3), characteristic dynamical charge (Z), and characteristic force constant (C in Hartree/bohr^2) for MO_6 and MO_8 structural units with M = (Hf, Zr, Ti), extracted from the calculations for the r-MO_2 structures on the one hand, and for the c-MO_2 and $MSiO_4$ structures on the other hand. (Note: The parameters extracted from the $MSiO_4$ structures take into account the values already obtained for SiO_4 SUs which are reported in table 7.)

	HfO_6	ZrO_6	TiO_6	HfO_8	ZrO_8	TiO_8
α	35.28	34.54	33.49	32.21	31.66	32.87
Z	7.19	7.45	8.59	6.77	6.95	7.70
C	0.1278	0.1050	0.0437	0.1630	0.1418	0.0778

four to eight between $x = 0$ and 0.5, with concentrations of ZrO_4 and ZrO_8 SUs varying at most quadratically. Note that the upper part of the band matches well the recent experimental data [72, 73]. The earlier data [68, 69, 75] cannot be explained. Figure 3 shows that, for a sufficient amount of ZrO_6 units, values of ϵ_0 at intermediate x can indeed be larger than estimated from a linear interpolation between SiO_2 and $ZrSiO_4$. However, in agreement with recent experiments [72, 73], the theory indicates that the extent of this effect is more limited than previously assumed [68–70].

The scheme of Rignanese *et al* [8] can also be applied to Hf and Ti silicates which are very similar to Zr silicates, provided that the value of the characteristic parameters are adapted. In this respect, the comparison between the various crystalline oxides and silicates carried out in the preceding sections provides very useful informations. Indeed, it is possible to extract the characteristic parameters of MO_6 and MO_8 SUs from the results obtained for the r-MO_2 structures on the one hand, and for the c-MO_2 and $MSiO_4$ structures on the other hand. These values are reported in table 8.

Note that the results in tables 7 and 8 for ZrO_6 and ZrO_8 structural units are in good agreement despite the fact they have been obtained using almost completely different sets of crystalline systems. The only common system is the zircon crystal. In table 7, the parameters are extracted from the results for crystalline systems that all include Si-centred SUs, whereas, in table 8, the reference crystals do not include such structural units (apart from zircon). This further increases the confidence in the validity of the scheme.

Basically, all the parameters in table 8 show a similar trend. On the one hand, the enhancement of the dielectric permittivities (both electronic and static) will be larger for the Ti-centred SUs than for Hf- and Zr-centred ones. On the other hand, the MO_6 units produce a larger enhancement than MO_8 units. Hence, for the amorphous silicates, the same kind of considerations should apply. In particular, for Ti amorphous silicates, the dielectric constants should be considerably larger than for Hf and Zr amorphous silicates. First, for Ti, the MO_6 SUs tend to be more stable (as in rutile) than the MO_8 ones, whereas, for Hf and Zr, the MO_8 SUs prevail. Second, all the characteristic parameters of Ti-centred SUs produce a larger enhancement than Hf and Zr ones.

5. Conclusions

This topical review has focused on the contribution of density functional theory to the study of the dielectric properties of crystalline and amorphous transition metal oxides and silicates considered as potential high-κ dielectrics. First, the principal equations of DFT related to the dielectric properties have been presented to allow for a thorough analysis of the results of the calculations. Then, the various studies existing in the literature have been discussed for group IVb M = (Hf, Zr, Ti) and IIIb M = (Y, La, Lu) transition metals crystalline oxides and/or silicates.

For the transition metals M = (Hf, Zr, Ti) belonging to group IVb, investigations have been reported on four crystalline phases of the dioxides MO_2 (cubic, tetragonal, monoclinic, and rutile) and on $MSiO_4$ crystalline silicates. A comparison between Hf, Zr, and Ti based oxides and silicates has been proposed. A globally increasing trend emerged for the static dielectric constant when substituting Hf by Zr, and Zr by Ti. This behaviour has been explained primarily in terms of the larger oscillator strengths.

The first-principles results for two crystalline phases (cubic and hexagonal) of sesquioxides M_2O_3 with M = Lu (group IIIb transition metal) have been summarized. Based on these calculations, it has been discussed that sesquioxides in the cubic structure (e.g. Y_2O_3 and Lu_2O_3) will consistently have dielectric constants smaller than those in the hexagonal structure (e.g. La_2O_3).

Finally, the dielectric properties of amorphous silicates have been discussed. A presentation has been given of a simple scheme, recently introduced, which connects the optical and static dielectric constants of the silicates to their underlying microscopic structure. The theory supports recent experiments which find a close to linear dependence of ϵ_0 on the Zr fraction x, and shows that higher dielectric constants can be achieved by increasing the concentration of ZrO_6 structural units. These results have been extended to Hf and Ti amorphous silicates. The predominance of MO_6 in the latter and the larger enhancement produced by Ti-centred structural units suggests that the dielectric constants should be considerably larger for Ti-based systems than for Hf and Zr ones.

Acknowledgments

The author wishes to thank Drs F Detraux, A Bongiorno, G Jun, and X Rocquefelte, as well as Professors K Cho, X Gonze, and A Pasquarello, who took an active part in the research leading to a great deal of the results presented in this topical review. The author is also grateful to P Delugas and V Fiorentini, as well as R B van Dover, for providing their results prior to publication. Support is acknowledged from the FNRS-Belgium, the FRFC project (No 2.4556.99), and the Belgian PAI-5/1/1. Last but not least, the author would like to acknowledge J Bouchet, F Detraux, X Gonze, and A Pasquarello for their suggestions after a careful reading of the manuscript.

References

[1] http://public.itrs.net
[2] Wilk G D, Wallace R M and Anthony J M 2001 *J. Appl. Phys.* **89** 5243–75
[3] Rignanese G-M, Gonze X and Pasquarello A 2001 *Phys. Rev.* B **63** 104305
[4] Rignanese G-M, Detraux F, Gonze X and Pasquarello A 2001 *Phys. Rev.* B **64** 134301
[5] Zhao X and Vanderbilt D 2002 *Phys. Rev.* B **65** 075105
[6] Zhao X and Vanderbilt D 2002 *Phys. Rev.* B **65** 233106
[7] Fiorentini V and Gulleri G 2002 *Phys. Rev. Lett.* **89** 266101
[8] Rignanese G-M, Detraux F, Gonze X, Bongiorno A and Pasquarello A 2002 *Phys. Rev. Lett.* **89** 117601
[9] Rignanese G-M, Gonze X, Jun G, Cho K and Pasquarello A 2004 *Phys. Rev.* B **69** 184301
[10] Rignanese G-M, Rocquefelte X, Gonze X and Pasquarello A 2005 *Int. J. Quantum Chem.* **101** 793–801
[11] Delugas P and Fiorentini V 2005 *Microelectron. Reliab.* at press
Bonera E, Scarel G, Fanciulli M, Delugas P and Fiorentini V 2005 *Phys. Rev. Lett.* **94** 027602
[12] Marsella L and Fiorentini V 2004 *Phys. Rev.* B **69** 172103
[13] Parlinski K, Li Z Q and Kawazoe Y 1997 *Phys. Rev. Lett.* **78** 4063–6
[14] Detraux F, Ghosez P and Gonze X 1998 *Phys. Rev. Lett.* **81** 3297
[15] Lee C, Ghosez P and Gonze X 1994 *Phys. Rev.* B **50** 13379–87
[16] Lee C Y and Gonze X 1994 *Phys. Rev.* B **49** 14730–1

[17] Králik B, Chang E K and Louie S G 1998 *Phys. Rev.* B **57** 7027–36
[18] Finnis M W, Paxton A T, Methfessel M and van Schilfgaarde M 1998 *Phys. Rev. Lett.* **81** 5149–52
[19] Jomard G, Petit T, Pasturel A, Magaud L, Kresse G and Hafner J 1999 *Phys. Rev.* B **59** 4044–52
[20] Lowther J E, Dewhurst J K, Leger J M and Haines J 1999 *Phys. Rev.* B **60** 14485–8
[21] Asahi R, Taga Y, Mannstadt W and Freeman A J 2000 *Phys. Rev.* B **61** 7459–65
[22] Mikami M, Nakamura S, Kitao O, Arakawa H and Gonze X 2000 *Japan. J. Appl. Phys.* 2 **39** L847–50
[23] Demkov A A 2001 *Phys. Status Solidi* b **226** 57–67
[24] Muscat J, Swamy V and Harrison N M 2002 *Phys. Rev.* B **65** 224112
[25] Mikami M, Nakamura S, Kitao O and Arakawa H 2002 *Phys. Rev.* B **66** 155213
[26] Xu Y N, Gu Z Q and Ching W Y 1997 *Phys. Rev.* B **56** 14993–5000
[27] Ching W Y, Ouyang L Z and Xu Y N 2003 *Phys. Rev.* B **67** 245108
[28] Vanderbilt D 1997 *Curr. Opin. Solid State Mater. Sci.* **2** 701–5
Ghosez P, Gonze X and Michenaud J-P 1997 *Ferroelectrics* **194** 39–54
George A M, Iniguez J and Bellaiche L 2001 *Nature* **413** 54–7
Sai N, Rabe K M and Vanderbilt D 2002 *Phys. Rev.* B **66** 104108
Veithen M and Ghosez P 2002 *Phys. Rev.* B **65** 214302
Hill N A 2002 *Annu. Rev. Mater. Res.* **32** 1–37
Cockayne E 2003 *J. Eur. Ceram. Soc.* **23** 2375–9
Bungaro C and Rabe K M 2004 *Phys. Rev.* B **69** 184101
Vanderbilt D 2004 *Ferroelectrics* **301** 9–14
Dieguez O, Tinte S, Antons A, Bungaro C, Neaton J B, Rabe K M and Vanderbilt D 2004 *Phys. Rev.* B **69** 212101
[29] Baroni S, de Gironcoli S, Corso A D and Giannozzi P 2001 *Rev. Mod. Phys.* **73** 515–62
[30] http://www.pwscf.org
[31] http://www.abinit.org
[32] Gonze X and Lee C 1997 *Phys. Rev.* B **55** 10355–68
[33] Gonze X, Beuken J-M, Caracas R, Detraux F, Fuchs M, Rignanese G-M, Sindic L, Verstraete M, Zerah G, Jollet F, Torrent M, Roy A, Mikami M, Ghosez P, Raty J-Y and Allan D C 2002 *Comput. Mater. Sci.* **25** 478–92
[34] Troullier N and Martins J L 1991 *Phys. Rev.* B **43** 1993–2006
[35] Teter M 1993 *Phys. Rev.* B **48** 5031–41
[36] Monkhorst H J and Pack J D 1976 *Phys. Rev.* B **13** 5188–92
[37] Hohenberg P and Kohn W 1964 *Phys. Rev.* **136** B864–71
[38] Kohn W and Sham L J 1965 *Phys. Rev.* **140** A1133–8
[39] Duran P and Pascual C 1984 *J. Mater. Sci.* **19** 1178–84
[40] Teufer G 1962 *Acta Crystallogr.* **15** 1187
[41] Ruh R, Garrett H J, Domagala R F and Tallen N M 1968 *J. Am. Ceram. Soc.* **51** 23–7
[42] Aldebert P and Traverse J P 1985 *J. Am. Ceram. Soc.* **68** 34–40
[43] Wang J, Li H P and Stevens R 1992 *J. Mater. Sci.* **27** 5397–430
[44] Adam J and Rogers M D 1959 *Acta Crystallogr.* **12** 951
[45] Abrahams S C and Bernstein J L 1971 *J. Chem. Phys.* **55** 3206–11
[46] Speer J A and Cooper B J 1982 *Am. Mineral.* **67** 804–8
[47] Mursic Z, Vogt T, Boysen H and Frey F 1992 *J. Appl. Crystallogr.* **25** 519–23
[48] Slater J C 1964 *J. Chem. Phys.* **39** 3199–204
[49] Lide D R 1995 *CRC Handbook for Chemistry and Physics* 76th edn (Boca Raton, FL: CRC Press)
[50] Little E J and Jones M M 1960 *J. Chem. Educ.* **37** 231–3
[51] Pecharromán C and Iglesias J E 1994 *Phys. Rev.* B **49** 7137–47
[52] Kukli K, Ihanus J, Ritala M and Leskela M 1996 *Appl. Phys. Lett.* **68** 3737–9
[53] Gusev E P, Cartier E, Buchanan D A, Gribelyuk M, Copel M, Okorn-Schmidt H and D'Emic C 2001 *Micorelectron. Eng.* **59** 341–9
[54] Liu D W, Perry C H and Ingel R P 1988 *J. Appl. Phys.* **64** 1413–7
[55] Wood D L and Nassau K 1982 *Appl. Opt.* **21** 2978–81
[56] Pecharromán C, Ocaña M and Serna C J 1996 *J. Appl. Phys.* **80** 3479–83
[57] French R H, Glass S J, Ohuchi F S, Xu Y N and Ching W Y 1994 *Phys. Rev.* B **49** 5133–42
[58] Lanagan M T, Yamamoto J K, Bhalla A and Sankar S G 1989 *Mater. Lett.* **7** 437–40
[59] Dwivedi A and Cormack A N 1990 *Phil. Mag.* **61** 1–22
[60] Buchanan R C (ed) 1986 *Ceramic Materials for Electronic* (New York: Dekker)
[61] Feinberg A and Perry C H 1981 *J. Phys. Chem. Solids* **42** 513–8

[62] Traylor J G, Smith H G, Nicklow R M and Wilkinson M K 1971 *Phys. Rev.* B **3** 3457–72
[63] Parker R A 1961 *Phys. Rev.* **124** 1719–22
[64] Samara G A and Peercy P S 1973 *Phys. Rev.* B **7** 1131–48
[65] Gervais F, Piriou B and Cabannes F 1973 *J. Phys. Chem. Solids* **34** 1785–96
[66] Pecharromán C, Ocaña M, Tartaj P and Serna C J 1994 *Mater. Res. Bull.* **29** 417–26
[67] Wyckoff R 1963 *Crystal Structures* vol 2 (New York: Wiley)
[68] Wilk G D and Wallace R M 2000 *Appl. Phys. Lett.* **76** 112–4
[69] Wilk G D, Wallace R M and Anthony J M 2000 *J. Appl. Phys.* **87** 484–92
[70] Lucovsky G and Rayner G B J 2000 *Appl. Phys. Lett.* **77** 2912–4
[71] Kurtz H A and Devine R A B 2001 *Appl. Phys. Lett.* **79** 2342–4
[72] Qi W J, Nieh R, Dharmarajan E, Lee B H, Jeon Y, Kang L, Onishi K and Lee J C 2000 *Appl. Phys. Lett.* **77** 1704–6
[73] van Dover R B, Manchanda L, Green M L, Wilk G, Garfunkel E and Busch B 2001 unpublished
[74] Nogami M 1985 *J. Non-Cryst. Solids* **69** 415–23
[75] Misra V 2001 unpublished
[76] Varshneya A K 1994 *Fundamental of Inorganic Glasses* (San Diego, CA: Academic)